# CHAPTER III

# FLUX-DENSITY MEASUREMENTS USING THE OOTY SYNTHESIS RADIO TELESCOPE

## 3.1: INTRODUCTION

In order to study low-frequency variability, it was decided to measure the flux density of a sample of compact radio sources every three months with a typical accuracy of ~ 5 %. Full synthesis mapping was not attempted because of the large number of sources in the sample. Also, such full mapping was not necessary, since we selected only those sources compact enough to be unresolved by the Ooty Synthesis Radio Telescope (OSRT) and were interested in measuring only their total flux densities. These observations could have been carried out with the Ooty Radio Telescope (ORT) alone were it not for its high confusion limit ($3\sigma$) of ~ 1.5 Jy. However, while use of the OSRT considerably reduced the confusion limit, it complicated both the observations and data analysis procedure.

This chapter begins with a calculation of the confusion limit for the ORT and we show how this is reduced for an aperture-synthesis instrument, naturally justifing the use of the OSRT for the present experiment. This is followed by brief descriptions of the basic principles of aperture-synthesis and the OSRT. The following section deals with the usual OSRT observing mode and data analysis and the problems that arises when these are applied to the observations of 'weak' sources over short time durations. Finally, we discuss the method actually adopted for the flux-density measurements and its limitations and accuracy.

## 3.2: CONFUSION LIMITS OF THE ORT AND THE OSRT

If a radio telescope is fixed and the sky is left to drift past it, a random fluctuating response is recorded. The stronger peaks, with a transit time characteristic of the telescope beamwidth, will be due to the passage of radio sources through the beam but the high-frequency smaller-magnitude fluctuations will be due to noise. Because of its random nature, time averaging reduces the noise in proportion to $1/\sqrt{T}$ where, T is the integration time. However, if we continue to increase T, the reduction of the ripple on the records ceases at a certain point and any further time-averaging does not improve the signal-to-noise ratio (SNR). The ripple at this point is caused predominantly by the background of radio sources passing through the main beam and the side-lobes of the antenna. If, for a particular observing mode (i.e. some specified integration time T), the rms value of these fluctuations is more than that of the thermal noise of the system, the telescope is said to be confusion limited.

One way of estimating the confusion limit ($3\sigma$) is to use the practical criterion that the average source density (in any survey) should not exceed one object in twenty-five beam-areas (Methods in Experimental Physics, Vol 12, Part C). The main-beam area of the ORT (for $0°$ declination) is

(i) in the total-power (TP) mode $= 1.133546 \times 2° \times 5'.6$

$= 6.445 \times 10^{-5}$ steradian

and (ii) in the correlator (or so-called

$$\text{phase-switched, } \phi\text{-Sw) mode} = 1.133546 \times 2^{\circ} \times 3'.6$$

$$= 4.144 \times 10^{-5} \text{ steradian}$$

-------(3.2.1)

One source per 25 beam areas requires that there should be about 620 and 965 sources per steradian down to the limiting flux densities in the TP and $\phi$-Sw modes respectively. Using the cumulative source count at 408 MHz. (Ryle, 1968) and assuming an average spectral index for the radio sources of 0.7 between 408 and 327 MHz, we find that this requirement determines the confusion limit to be 1.59 and 1.17 Jy for the TP and $\phi$-Sw mode respectively. This is not an exact estimate as we have neglected the effect of the side lobes which will be more pronounced for $\phi$-Sw operation. Since this is a $3\sigma$ limit, the r.m.s. contribution to the noise from main-beam confusion amounts to about 500 and 234 mJy for the TP and $\phi$-Sw modes respectively. In comparision, the thermal noise for a 1 sec integration is normally about 140 mJy. At this point, one might argue that since the confusion remains unchanged in an equatorial antenna for a particular source (field), it should not affect any variability study. However, the feed line of the ORT consists of 1056 dipoles, all of which have to be consistently phased to maintain a particular beam shape. Hence there is a likelihood of considerable apparent flux-density variations to be caused by secular changes in the beam shape, which could have different variations for different declinations.

Confusion noise in the OSRT

Perley and Erickson (1984) have calculated the rms noise in a complex correlator due to the passage of a large number of background sources through the interferometer fringe pattern. For a particular baseline, this is given by

$$\sigma^2_{con} = 0.5 \left[\int S^2 \; n(S) \; dS\right] \left[\int P^2 \; d\Omega \;\right] \qquad \text{-------(3.2.2)}$$

where, $n(S)$ = the differential number count of radio sources within the flux density range S to S+dS

and $P$ = the synthesised beam

The second moment of the differential number count can be estimated using a relation ( Sukumar et al., 1988),

$$\int S^2 \; n(S) \; dS = 1637 \; F^{2\beta} \; (1.247)^6 = 7186.64 \; Jy^2 \; ster^{-1} \qquad \text{------(3.2.3)}$$

where, $F = 408/\nu$ (MHz)

and $\beta$ = the index of Log N - Log S distribution

= 0.7

As discussed below, the adopted observing method restricted the field of view for the present observation to 2° x 7' (as compared to the usual field of view of the OSRT of 2° x 42'). Since a multi-element interferometer measures the visibility at different U-V spacings, the noise contributions due to confusion are summed with random phase, whereas the signal from the source at the phase centre adds in phase. Hence, if N independent points are averaged, confusion, like the thermal noise, gets reduced by a factor of $1/\sqrt{N}$ . In the present application, we have taken vector-averages of the visibility points from four baselines over 5 minutes (for reasons discussed below). The OSRT measures one visibility point per min and hence, N = 20 (assuming there is an independent point per min) in this case.

$$\text{Therefore,} \quad \sigma^2_{con}\ (\text{OSRT}) = \frac{1}{\sqrt{20}}\left[0.5 \times 7186.64 \times 2 \times (7/60) \times (\pi/180)^2\right]$$

$$= 110 \text{ mJy} \qquad \text{-------}(3.2.4)$$

This is consistent with the value of ~ 3 mJy for a 9-hr integration, as quoted by Sukumar et al.(1988). Thus, in this method, the contribution of confusion is reduced by a considerable amount.

## 3.3: BASIC PRINCIPLES OF APERTURE SYNTHESIS AND THE OSRT

Let us consider a distant source, subdivided into infinitesimal elements of solid angle each with a brightness $B_i$. Each of these source elements generates Huygens wavelets which can be considered to be plane waves at the distance of the observer. Since these plane waves are coming from various directions, their sum is a complex phasor, $\varepsilon(\ell,m)$, which represents an "angular spectrum" of plane waves. The observer will note that in the plane (x,y) perpendicular to the observer-source line, the electric field E(x,y) produced by the source with direction cosines $(\ell,m)$ will vary with the position in the plane. Booker and Clemmow (1950) proved that the angular spectrum and the field distribution are related by a Fourier Transform relation

$$E(x,y) = \int\int_{-\infty}^{+\infty} \varepsilon(\ell,m) \exp\left[ j \frac{2\pi}{\lambda} (x\ell+ym)\right] d\ell\, dm \qquad \text{------}(3.3.1)$$

(neglecting sky curvature)

Conventionally, we consider $u = x/\lambda$ and $v = y/\lambda$ so that

$$E(u,v) = \int\int_{-\infty}^{+\infty} \varepsilon(\ell,m) \exp\left[ j2\pi(u\ell+vm)\right] d\ell\, dm \qquad \text{------}(3.3.2)$$

The required quantity is the intensity (or brightness) distribution over the source, $B(\theta,\phi)$. The solid angle subtended by any source element is $d\ell dm$ and the brightness of that element in the direction $(\ell,m,)$ is proportional to $|\varepsilon(\ell,m)|^2$. Hence, the brightness distribution can be written as

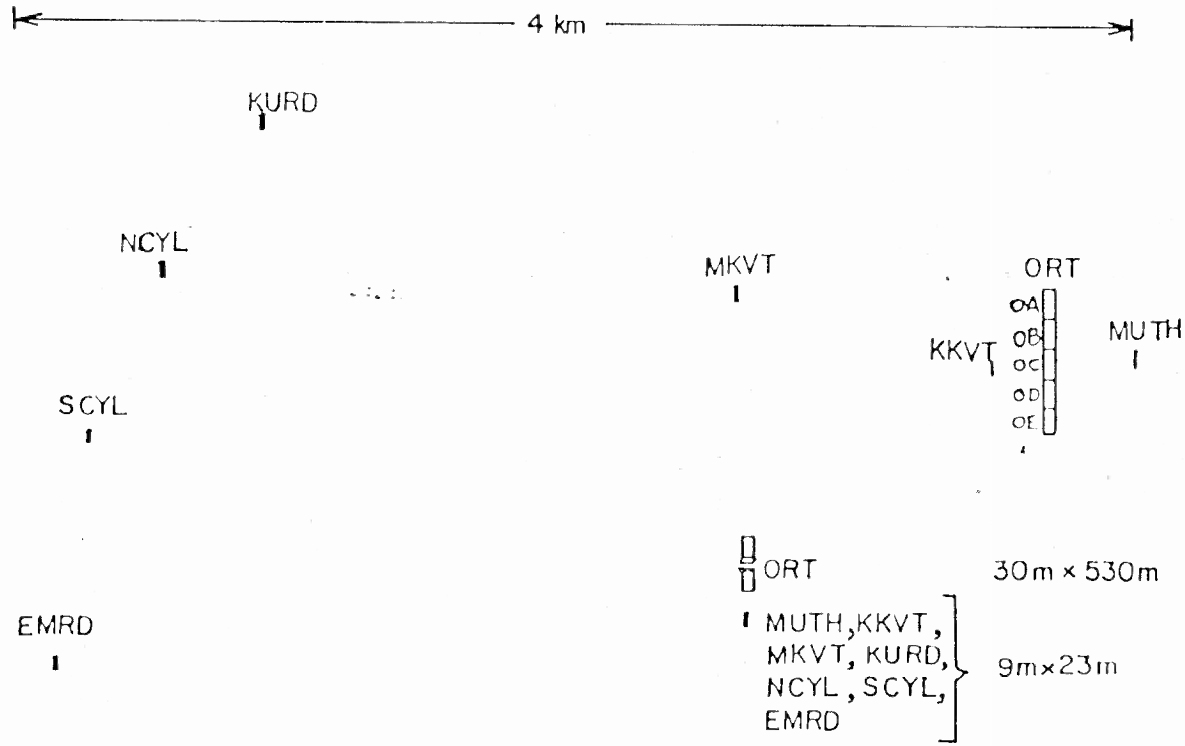


Fig.III-1: Lay out of OSRT antennas

Table III-1: Some useful parameters of the OSRT

| | |
|---|---|
| Antennae | Five ORT sections (each 92m X 30 m), OA,OB,OC,OD,OE. Seven smaller parabolic cylinders ('baby cylinders') each with dimensions 23m X 9 m. |
| Maximum baseline | 4 km (EW) X 2 km (NS). |
| Frequency | 327 MHz. |
| Bandwidth | 4 MHz. |
| Sky coverage : HA | $-04^h\ 07^m$ to $+05^h\ 26^m$ for ORT-sections<br>$-05^h\ 30^m$ to $+05^h\ 30^m$ for the baby cylinders. |
| DEC | $\pm 50°$ |
| Field of view | 124' X 31' for the baselines involving ORT-sections.<br>170' X 42' for baselines between the baby cylinders and the ORT-sections |
| Synthesised beamwidth | $40''$ X $90''$ at 0° declination. |
| Sensitivity | 15 mJy/Beam ($5\sigma$) for 9 hr integration. |

$$B(\theta,\phi) = \varepsilon(l,m)\ \varepsilon^*(l,m) \qquad \text{-------(3.3.3)}$$

The lateral coherence function of the electric field is defined as

$$\Gamma(u,v) = \langle\ E(u,v)\ E^*(u+u',v+v')\ \rangle \qquad \text{-------(3.3.4)}$$

where, < > denotes averaging over all values of u',v'. Using the Wiener-Kinchin theorem, which can be stated as:

If, $G(s) \overset{F.T.}{\Rightarrow} g(x)$

and, $H(a) = \langle g(x)\ g^*(x-a)\rangle$ then the Fourier transform of H(a) is given by

$$\int_{-\infty}^{+\infty} H(a)\exp(-2\pi jsa)\ da = |G(s)|^2 \qquad \text{-------(3.3.5)}$$

and taking a Fourier transform of (3.3.4), we get

$$\int_{-\infty}^{+\infty} \Gamma(u,v)\exp -2\pi j(u\ell+vm)\ du\ dv = |\varepsilon(\ell,m)|^2 = B(\theta,\phi) \qquad \text{-----(3.3.6)}$$

Thus, the brightness distribution and the lateral coherence function of the electric field are related by a Fourier transform relation. In an aperture- synthesis instrument, we measure the normalized lateral-coherence or 'visibility', defined by:

$$V(u,v) = \frac{\langle\ E(u',v')\ E^*(u'+u,v'+v)\ \rangle}{\langle\ |E(u',v')|^2\ \rangle} \qquad \text{------(3.3.7)}$$

for a large number of u,v values (baseline vector $\overline{b} = \overline{u}+\overline{v}$). Then, using an inverse Fourier transform, we can reconstruct the sky-brightness distribution, $B(\theta,\phi)$.

**THE OSRT:**

The Ooty Synthesis Radio Telescope (OSRT) consists of a 30 x 530 $m^2$ parabolic-cylindrical antenna, the ORT (Swarup et al., 1971), and seven and a detailed description is given by Sukumar et al. (1988).

The feed-line of the ORT consists of an array of 1056 collinear dipoles and is grouped into 22 modules containing 48 dipoles each. For use in the OSRT, The ORT is sub-divided into five segments which are treated as five individual elements of the synthesis array (named OA, OB, OC, OD and OE). Each segment consists of 4 modules (the northern and southern-most modules being excluded). The signal received by each module at 326.5 MHz is amplified and down-converted to 30 MHz using a local oscillator (LO) signal at 296.5 MHz. This is brought to the central receiving room through underground cables. The dipole array and receiver electronics for the smaller antennas are similar to those of the ORT.

All the antennas are equatorially mounted and are mechanically steerable in hour-angle (some relevant parameters for the OSRT are listed in Table III-1). Declination pointing is achieved by properly phasing the dipoles in the feed lines using 4-bit diode-controlled phase-shifters placed after each dipole. The positioning in hour angle and declination of all the antennas and the monitoring of the status of the electrical and electronic systems at the remote stations are achieved by means of a computer-controlled RF telemetry system which employs VHF and cable links to the central control room.

Local-oscillator signals at 296.5 MHz are transmitted from the control room to the nearby (up to distances of ~ 300 m) antenna by underground cables. For the more distant antennas, the coherent LO signal are generated from the master oscillator using phase-locked loops at the remote stations.

The 30-MHz IF signals (over bandwidths of 4 MHz) from the remote stations are brought to the central receiving room using cable and microwave links. These are then down-converted to video signals and fed through automatic level controllers (ALC) to the 256-channel digital delay line correlator unit (DDLC) which compensates the geometric delays with respect to a phase-reference point at the centre of the ORT element OC, fringe-stopping and the formation of the visibility function. The on-line PDP 11/24 mini-computer (which also controls the antennas and sets the delays) reads and stores the sine and the cosine correlator outputs of each DDLC channel every six seconds through the DR11C interfaces.

The off-line data analysis is performed using locally-developed software in the PDP 11/70 computer and the AIPS package installed on the VAX 11/750 computer. Firstly, the 6-sec data points for a particular source are added vectorially to obtain 1-min data averages. Phase corrections to compensate for atmospheric refraction (Sukumar, 1986) are then applied to these. Usually, a nearby point source with accurately-known position and flux density is observed every 15-20 min. Using the visibility data for this calibrator source, antenna-based amplitude and phase gain factors are calculated. With the assumption that the system and the atmospheric conditions vary only linearly between two successive scans on the calibrator, interpolation of the gain factors gives the appropriate factors to be applied to the source data. After calibration, the visibility amplitudes are expressed in units of Jy, while the phase values are relative to a point at the field centre. The calibrated data are then Fourier transformed and CLEANed to produce the final map.

For a full OSRT synthesis observation of 9 hr, a fairly good uv-coverage can be obtained. The equatorial (geomagnetic) ionospheric phase fluctuations which is a major problem at Ooty because of its proximity to the Geomagnetic equator, can be corrected for using a self-calibration technique for strong ($S_{327} > 5$ Jy) sources, leading to improved dynamic range.

## 3.4:Difficulties in adopting the normal observing mode for flux-density monitoring

With the large number of sources to be monitored every 3-months, it was impractical to observe each source for 9 hr. In practise, we could spend about 2 hr on each source per observation. The expected 327-MHz flux densities of most sources in the programme were about 1 Jy and it was difficult to find a nearby calibration source for each. These constraints gave rise to the following difficulties with the standard mode of observations.

### (A) The effect of ionospheric phase fluctuations:

The ionospheric phase fluctuations affected the interferometric measurements in two ways, depending upon whether the baseline involved was longer or shorter than the correlation length of the phase fluctuations. The fluctuations along an initially plane wavefront, distorted by traversing an irregular medium, can be characterized by the 'structure function' of phase, defined by:

$$D(b) = \langle [\, \phi(x) - \phi(x-b)]^2 \rangle \qquad \text{-------}(3.4.1)$$

where, b represents the projected baseline of an interferometer. The rms deviation in the visibility phase (for that baseline) is given by

$$\sigma_\phi(b) = \sqrt{D(b)} \qquad \text{-------}(3.4.2)$$

Depending upon the scale-sizes of the irregularities in the ionosphere, there exists a maximum separation $d_m$, for baselines shorter than which

$$\sigma_\phi = \frac{2\pi}{\lambda}\, a\, b^\beta, \quad \text{for } b < d_m$$

where, a is a constant ------(3.4.3)

while, $\sigma_\phi = \sigma_m$, and is constant for $d \geq d_m$

The value of $d_m$ for the ionosphere has been found to be $\approx$ 5 km (Ratcliffe,1956)

For baselines shorter than $d_m$, the measured visbility is related to the true visibility by the equation,

$$V_m = V_t \exp(j\phi) \qquad \text{------(3.4.4)}$$

where, $\phi$ is a Gaussian random variable with zero mean and the expectation value of the measured visibility

$$\langle V_m\rangle = V_t \langle\exp(j\phi)\rangle = V_t \exp(-\sigma_\phi{}^2/2) \qquad \text{-------(3.4.5)}$$

If we assume $\beta = 1$, then using eqn. (3.4.3) we get

$$\langle V_m\rangle = V_t \exp(-2\pi^2 a^2 q^2) \qquad \text{-------(3.4.6)}$$

where, q is the magnitude of the projected baseline vector, $\bar{b}$ in units of $\lambda$. Therefore, in this case the visibility is multiplied by a Gaussian function, the ionospheric weighting funtion,

$$W(q) = \exp(-2\pi^2 a^2 q^2) \qquad \text{------(3.4.7)}$$

The map generated by the Fourier transformation of eqn.(3.3.6) is then convolved by the Fourier transform of W(q),

$$W(\theta) \propto \exp(-\theta^2/2a^2) \qquad \text{-------(3.4.8)}$$

The effect would be that the source is broadened and the resolution limited by 'seeing' [For other values of $\beta$, W(q) can be calculated either analytically or numerically].

For baselines where $b \geq d_m$, two situations may arise:

(1) if the time-scale of phase fluctuations is shorter than the measurement interval, all the visibility measurements will be reduced by a constant factor, $\exp(-\sigma_m^2/2)$. Resolution will not be degraded in this

(a)

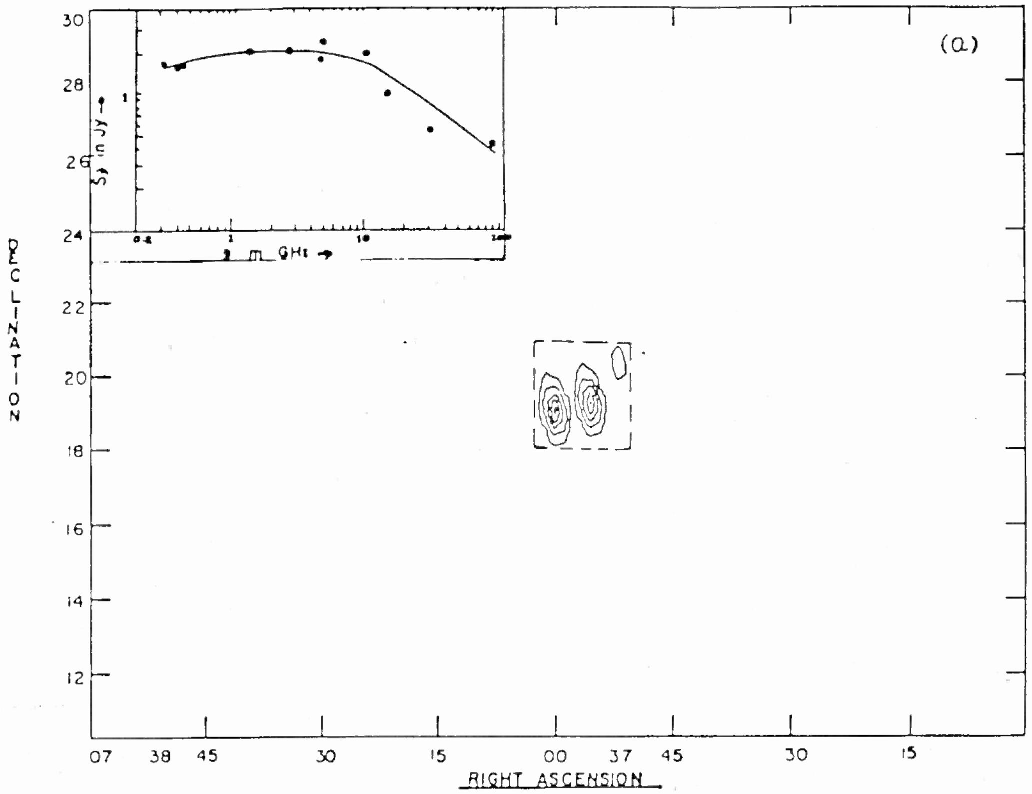


PEAK FLUX = 4·0265E-01 JY/BEAM
LEVS = 7·5000E-02 * (-3·00, -2·00, -1·00, 1·000, 2·000, 3·000, 4·000, 5·000)

(b)

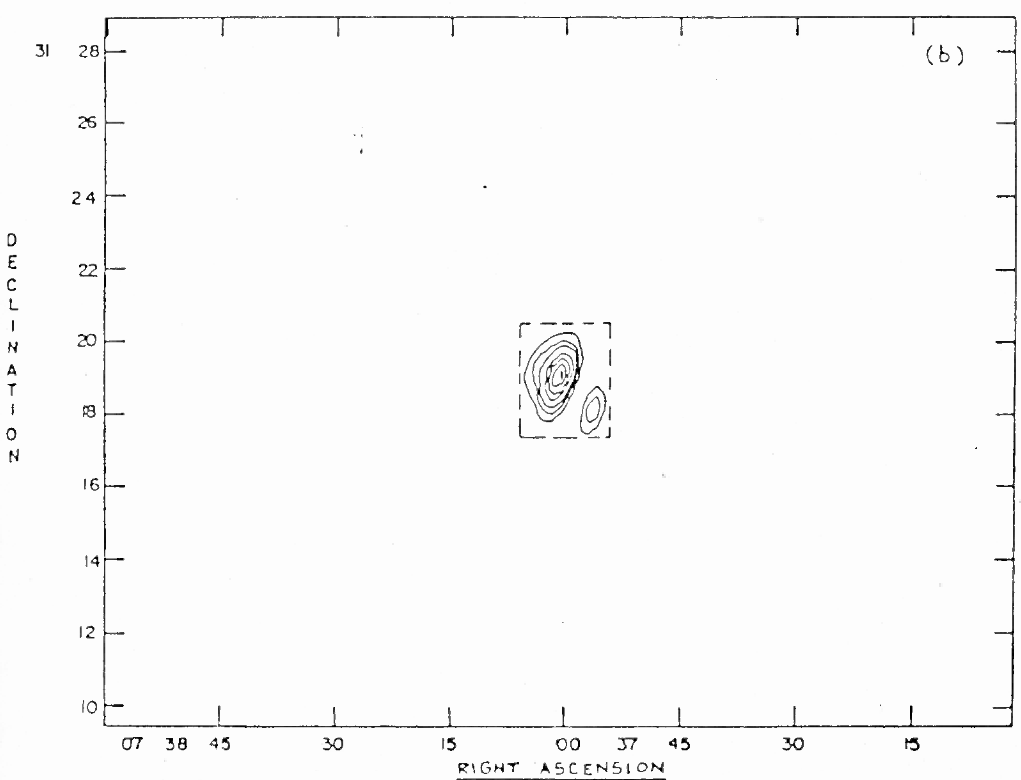


PEAK FLUX = 6·0194E-01 JY/BEAM
LEVS = 5·4000E-02 × (-3·00, -2·00, -1·00, 1·00, 2·00, 3·00, 5·00, 7·00, 9·00, 11·00)

Fig. III-2a,b: The effect of ionospheric phase fluctuations in OSRT 'snap-shot' maps.

case, although the flux density will be underestimated by a factor $\exp(-\sigma_m^2/2)$.

(2) when the time-scale of phase fluctuations is longer than the measurement intervals, each visibility value will suffer a phase error, $e^{j\phi}$, which is time-varying but whose statistics are independent of the baseline $\bar{b}$. If there are N measurements of a point source of flux density S, the map can be expressed as:

$$I(\theta_x, \theta_y) = \frac{S}{N} \sum_{i=1}^{N} e^{j\phi_i} \exp[2\pi j(\theta_x u_i + \theta_y v_i)] \qquad \text{------(3.4.9)}$$

The expectation value at the field centre is

$$\langle I(0,0) \rangle = S\, e^{-\sigma_m^2/2} \qquad \text{------(3.4.10)}$$

The flux-density measured at the peak response is underestimated with a rms deviation of $\sigma_s$ from its true value where,

$$\sigma_s = \frac{S}{\sqrt{N}} \sqrt{\left( 1 - \exp(-\sigma_m^2) \right)} \qquad \text{-------(3.4.11)}$$

The 'missing flux density' can be obtained by ignoring the thermal noise and averaging the amplitudes over the map if there is no other source within the field.

The situation usually encountered with the OSRT 4-km baselines is that described in case (2). Thus the estimated flux density from the peak value at the phase centre is an underestimate when the data are uncorrected for phase errors. Also, as the rms deviation $\sigma_s$ depends upon ionospheric conditions, it is time dependent. As an illustration of this uncertainty, we present in Fig.III-2a and 2b two maps of the compact source 0738+313 as observed on two consecutive days (22 and 23 April 1985). The source 0758+14 was used as a calibrator. On both days, four scans of 30 min duration each were taken on the source, with interleaved 5-min scans on the calibrator. The maps show clearly the effects of phase errors. The source 0738+313 is a compact flat-spectrum (Fig.III-2a inset) low-optical-polarization quasar which is used as an L and C-band calibrator at the VLA. Hence, it should be completely unresolved by the OSRT (synthesised HPBW = 148x 22arcsec at 16°). The total expected flux density at 327 MHz is ~ 1.6 Jy. In Figs III-2a and b, we see that the source is broken up into several components with the peak flux density changing from 0.6 Jy on 22nd April to 0.4 Jy on the 23rd. Integrated flux densities over the boxes indicated are 1.34 and 1.13 Jy respectively - a difference of ~ 20 %. The use of self-calibration technique would have been beneficial here, but it could not be applied for the following reasons,

(i) for a source of ~ 1 Jy strength, the signal-to-noise ratio for the correlations betweeen any two of the smaller antennas (baby-cylinders) are so poor (SNR < 1) compared to the ORT-baby or inter-ORT-element correlations that they had to be excluded. This led to non-closure conditions for the antenna gain equations.

(ii) The ORT-elements and the baby-cylinders have very different fields of view and contributedifferent levels of confusion, generating large baseline-dependent errors.

(B) The problems of amplitude calibration :

The amplitudes of the antenna-based gain factors of the OSRT elements are declination dependent. For the symmetric parabolic cylinders (seven 'baby cylinders'), the signal received through the back-lobe of the feed line interferes with that received by the front lobe. Therefore, the net power has a different declination dependence than just the projection

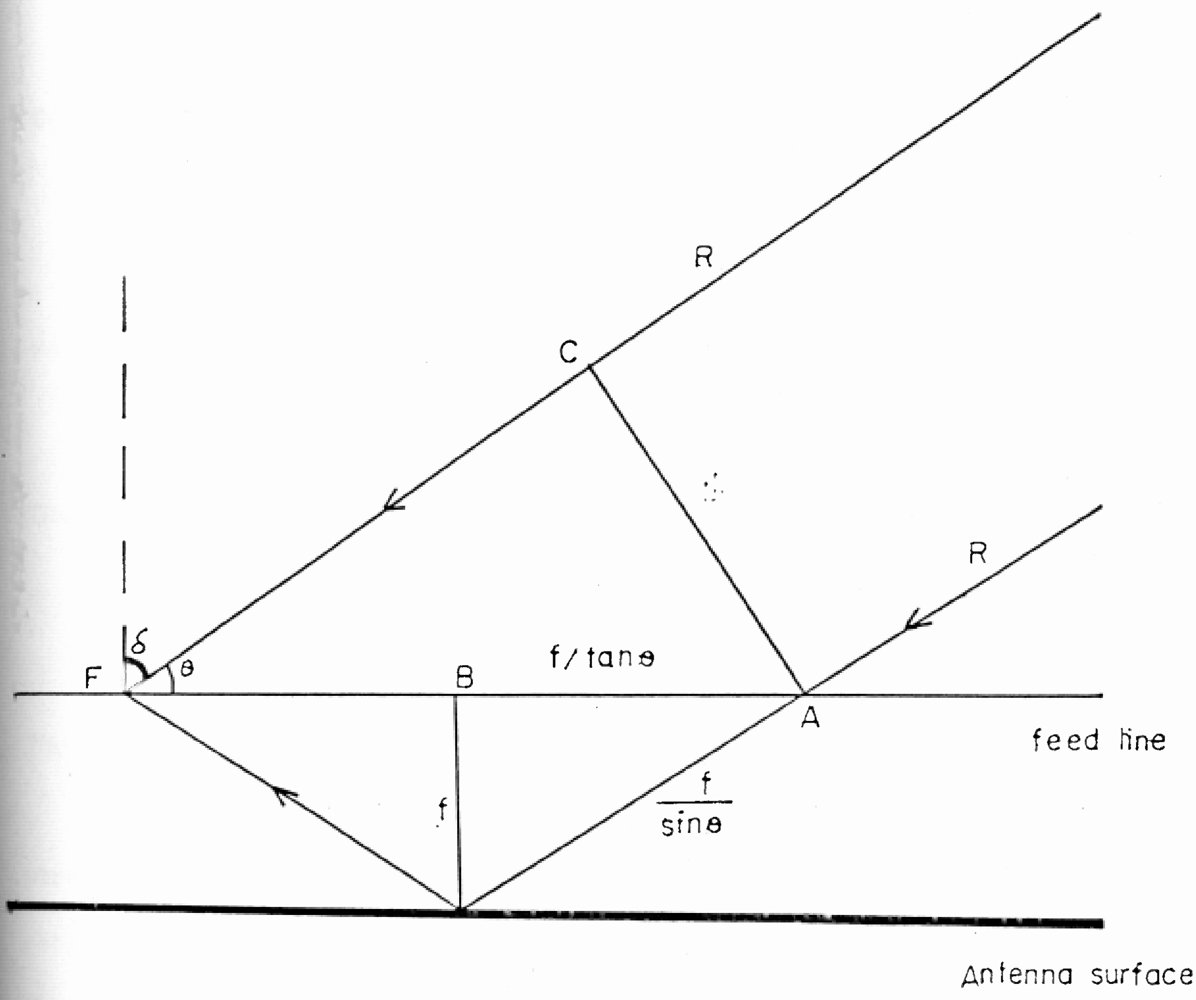


Fig. III-3: 'Back-lobe effect' in the symmetric cylinders.

effect. In Fig.III-3, we represent the ray received through the back-lobe by $R_1$ and that through the front lobe by $R_2$ with voltage gains $A_1$ and $A_2$ respectively.

The phase difference between $R_1$ and $R_2$ is given by:

$$\Delta\phi = \frac{2\pi}{\lambda} [ AO + OF - FC ] \qquad \text{-------(3.4.12)}$$

Geometrically, $FC = FA \cos\theta = 2\,AB \cos\theta = \frac{2f}{\tan\theta} \cos\theta = 2f \cos^2\theta/\sin\theta$

where, f is the focal length of the antenna

and, $OA + OF = \frac{2f}{\sin\theta}$

$$\text{Hence,} \quad \Delta\phi = \frac{2\pi}{\lambda} \cdot \left[\frac{2f}{\sin\theta} (1-\cos^2\theta)\right] = \frac{4\pi}{\lambda} f \cos\delta \qquad \text{-----(3.4.13)}$$

where, $\delta$ is the declination of the source $= 90 - \theta$

The net voltage received, $\bar{V} = A_2 \exp[i(wt + \phi + \Delta\phi)] + A_1 \exp[i(wt + \phi)]$

$$= A_2 \exp[i(wt + \phi + \Delta\phi)] \left[ 1 + G_b \exp(-i\,\Delta\phi) \right] \qquad \text{-----(3.4.14)}$$

where, $G_b = A_1/A_2$ = relative back-lobe gain

The received power $= \bar{V}\,\bar{V}^*$

$$= |A_0|^2 \cos\delta \left[1 + G_b^2 + 2G_b \cos(\frac{4\pi}{\lambda} f \cos\delta)\right] \qquad \text{---(3.4.15)}$$

whre the "cos $\delta$" term is introduced as both the feed line and the main reflector fore-shorten as cos $\delta$.

Therefore, the amplitude gain factor has the following declination dependence

$$g_x = A_x \left\{ \cos\delta \left[ 1 + G_b^2 + 2G_b \cos(\frac{4\pi}{\lambda} f \cos\delta \right] \right\}^{1/2} \qquad \text{----(3.4.16)}$$

where, $A_x$ is a normalizing constant the value of which depends upon the effective area of an antenna at the equator.

As the ORT-elements are assymmetric (the cross-section being a half parabola), the back-lobe does not contribute and the amplitude gain varies with declination as:

$$g_{oi} = A_{oi} (\cos\delta)^{1/2} \qquad \text{------(3.4.17)}$$

In order to verify eqns. (3.4.16) and (3.4.17) we have estimated the antenna-based amplitude gain factors for 30 calibration sources distributed over the declination range, $-40° < \delta < +50°$. Figs.III-4a-h show least-square fits of equations (3.4.16) and (3.4.17) to the gain factors derived from these observations as a function of declination. Although the mathematical form of this dependence can be calculated as above, in actual observing situations the dependence could be different because of the finite probability of malfunctions of some of the diode phase-shifters in the dipole array. Hence, the declination dependence of the amplitude gain factors has to be established for each observing run, unless a calibration source is found exactly at the same declination as the source. However, the use of just a single calibrator may lead to artificial variability since many calibrators are themselves compact sources (the chosen calibrators, nevertheless, have steep-radio-spectra) and are likely to be variables.

## 3.5: The Adopted Methodology

The above difficulties led us to measure the flux density with only a minimal use of the visibility phase and a different amplitude calibration procedure. The method is based on the principle of broken-coherence averaging (Thompson, Moran and Swenson, 1986), as is frequently used in VLBI data analysis. Essentially, the procedure involves the computation of the mean square value of a series of coherent measurements of fringe amplitudes, each made over a time shorter than the coherence-time.

The coherence time of an interferometer can be taken as the time over which the rms phase noise is less than 1 radian. The phase stability is normally characterised by a quantity called the Allan-variance which is

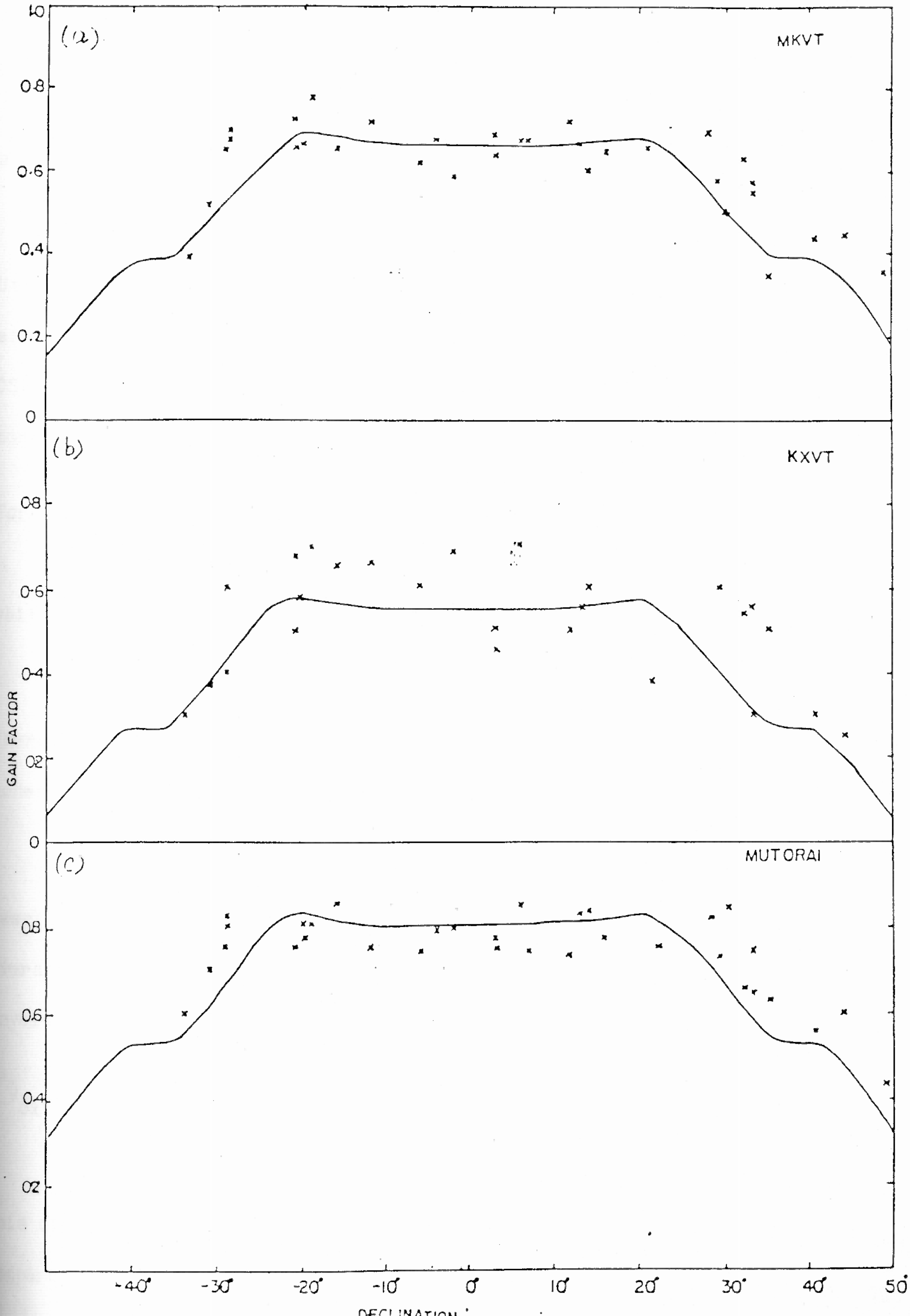


Fig. III-4: Declination dependence of the voltage-gain factors for OSRT antennas.

defined as:

$$\sigma^2_{\phi}(\tau) = \langle |\phi(t+2\tau) - 2\phi(t+\tau) + \phi(t)|^2 \rangle \quad \text{-----}(3.5.1)$$

and the definition of the coherence-time ($\tau_c$) can be expressed as

$$\sigma_{\phi}(\tau) = 1 \text{ radian} \quad \text{------}(3.5.2)$$

Using visibility phase values recorded on the point source 3C 286, we have estimated the Allan standard deviation ($\sigma_{\phi}$) for different baselines of the OSRT for various values of $\tau$ and estimated the corresponding coherence times.

For baselines involving the ORT elements:

$$\tau_c \approx 2 \text{ hr}$$

while, for the 4-km baselines: ------(3.5.3)

$$\tau_c \approx 10 \text{ min}$$

Therefore, we could add the visibility amplitudes of the 4-km baselines coherently for 5 minutes, even without any phase calibration.

To reduce the effects of confusion, the complex visibilities for baselines involving one 4-km antenna and all the five ORT-elements were averaged vectorially to generate the visibility points for a baseline involving a baby-cylinder and the whole of the ORT,

$$\bar{V}_{ox} = \frac{1}{5} \sum_{i=1}^{5} \bar{V}_{o_i x}, \quad \text{where, 'o}_i\text{' represents an ORT-element} \quad \text{---}(3.5.4)$$

and 'x' represents a 4-km antenna

This operation reduced the field of view for each baseline to 2° X 7', as compared to 2° X 42' in the case of the normal OSRT configuration. The averaging required a phase calibration which was achieved using a set of calibrators at least one of which was observed about once per two hours.

A least-square technique, identical to ANTSOL in the VLA calibration software, was used to determine the antenna-based phase calibrations as a function of time. This was then interpolated to find the appropriate corrections for the sources. Considering the longer coherence time for the inter ORT-element baselines, this method resulted in a good phase calibration for the ORT-elements. It was then possible to perform the vector averaging described by eqn. (3.5.4) and generate visibility points between the complete ORT and a 4-km antenna baseline (ox).

Assuming that the shape of the theoretical gain-declination curves [eqn. (3.4.16) and (3.4.17)] do not change, from the observations of the above-mentioned set of calibrators we have fitted the theoretical curves to the derived antenna-gain-parameters by changing only the normalizing constants ($A_x$ and $A_o$) for each antenna. The appropriate fitted curves were used for gain calibration in each particular observing session. The advantage of this procedure is that the goodness of these fits could be used as indicators of the conditions of the antennae and also the measured flux densities are not critically dependent on the assumed flux density of any particular calibration source. The flux density of individual calibrators can differ from the expected value either due to variability or due to errors. However, so long as the mean value of the differences is close to zero, there will be no systematic error in the estimated flux densities of the sources.

After calibrating the amplitudes of the vector-averaged (over five minutes) visibilities for the effective baselines between four 4-km antennas and the complete ORT ($\bar{V}_{ox}$), they are scalar averaged to obtain an estimate of the source flux density.

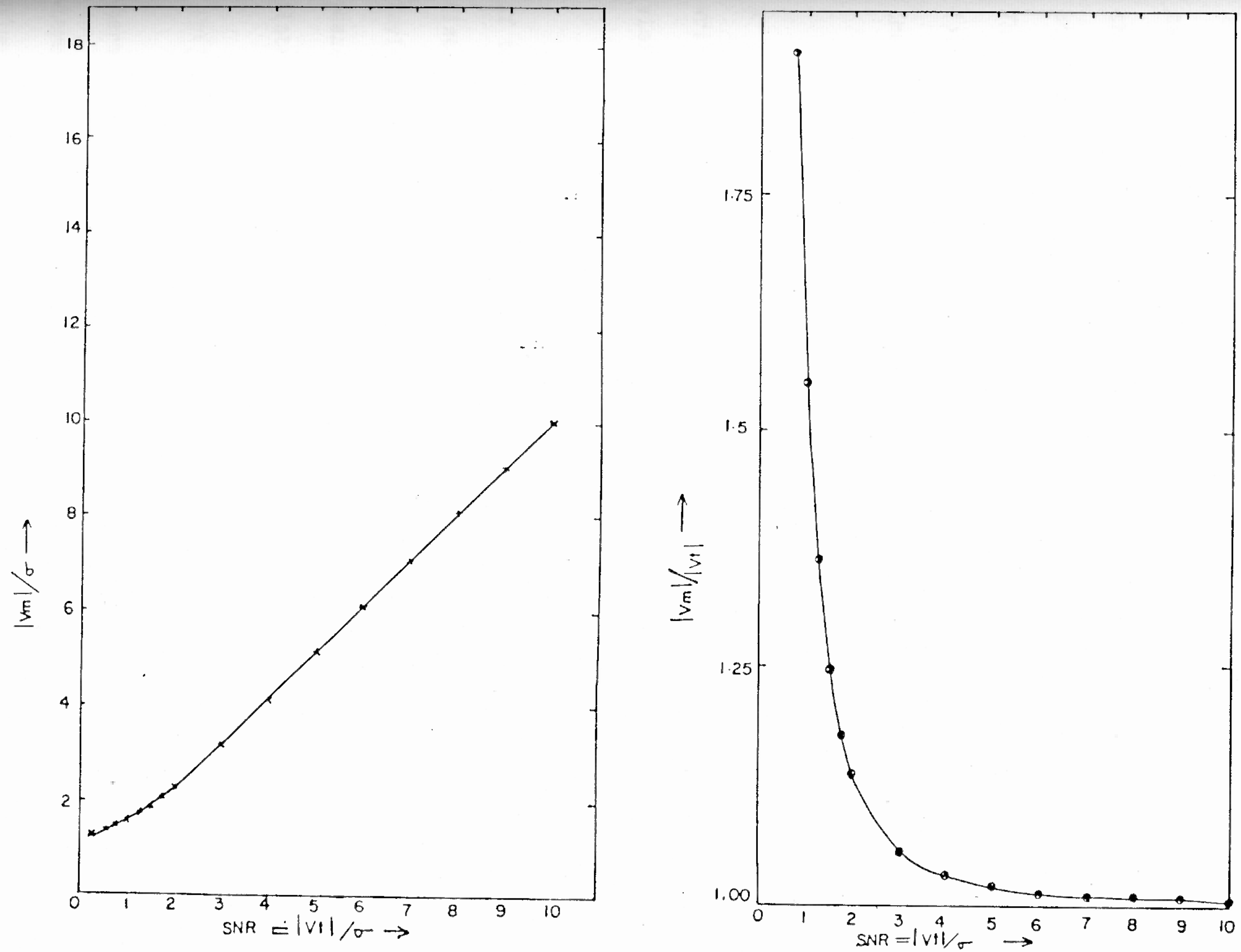


Fig. III-5a,b: The effect of noise bias in incoherent averaging of visibility amplitude (see text).

## 3.6: Limitations, Corrections and Errors .

(A) As no maps were made, any additional source within the $2° \times 7'$-sized field of view would get added to the flux density of the target source at the phase centre. To avoid such a situation, we searched the Molonglo Master Catalogue (Little et al., 1978) and excluded those sources which have a neighbouring source of strength $\geq 0.7$ Jy at 408 MHz. This limits the applicability of the method to relatively strong sources (>1 Jy) as the probability of finding a neighbouring source increases with the lowering of the flux density limit.

(B) Since we are using only the visibility amplitudes, there will be a positive bias due to noise in our estimated flux densities. We can write the measured complex visibility as the vector sum of the true visibility and the system noise ($\bar{\varepsilon}$)

$$\bar{V}_m = \bar{V}_t + \bar{\varepsilon} \qquad \text{-------(3.6.1)}$$

If the real and the imaginary parts of the noise have Gaussian probability distributions with zero means and rms deviations, $\sigma$ [or equivalently, a Rayleigh distribution for the amplitude and a uniform distribution for the phase], the probability distribution of the amplitude of $\bar{V}_m$ will be a Rice distribution (Papoulis, 1965):

$$p(|V_m|) = \frac{|V_m|}{\sigma^2} \exp\left(-\frac{|V_m|^2 + |V_t|^2}{2\sigma^2}\right) I_0\left(\frac{|V_m||V_t|}{\sigma^2}\right) \qquad \text{----(3.6.2)}$$

where, $I_0$ is the modified Bessel function of order zero. For the case where $\bar{V}_t$ has zero phase (point source at the phase centre) the expectation value of $|V_m|$ is:

$$\langle|V_m|\rangle = \frac{\sqrt{\pi}}{2}\sigma \exp\left(-\frac{|V_t|^2}{4\sigma^2}\right)\left[\left(1 + \frac{|V_t|^2}{2\sigma^2}\right) I_0\left(\frac{|V_t|^2}{4\sigma^2}\right) + \frac{|V_t|^2}{2\sigma^2} I_1\left(\frac{|V_t|^2}{4\sigma^2}\right)\right] \qquad \text{--(3.6.3)}$$

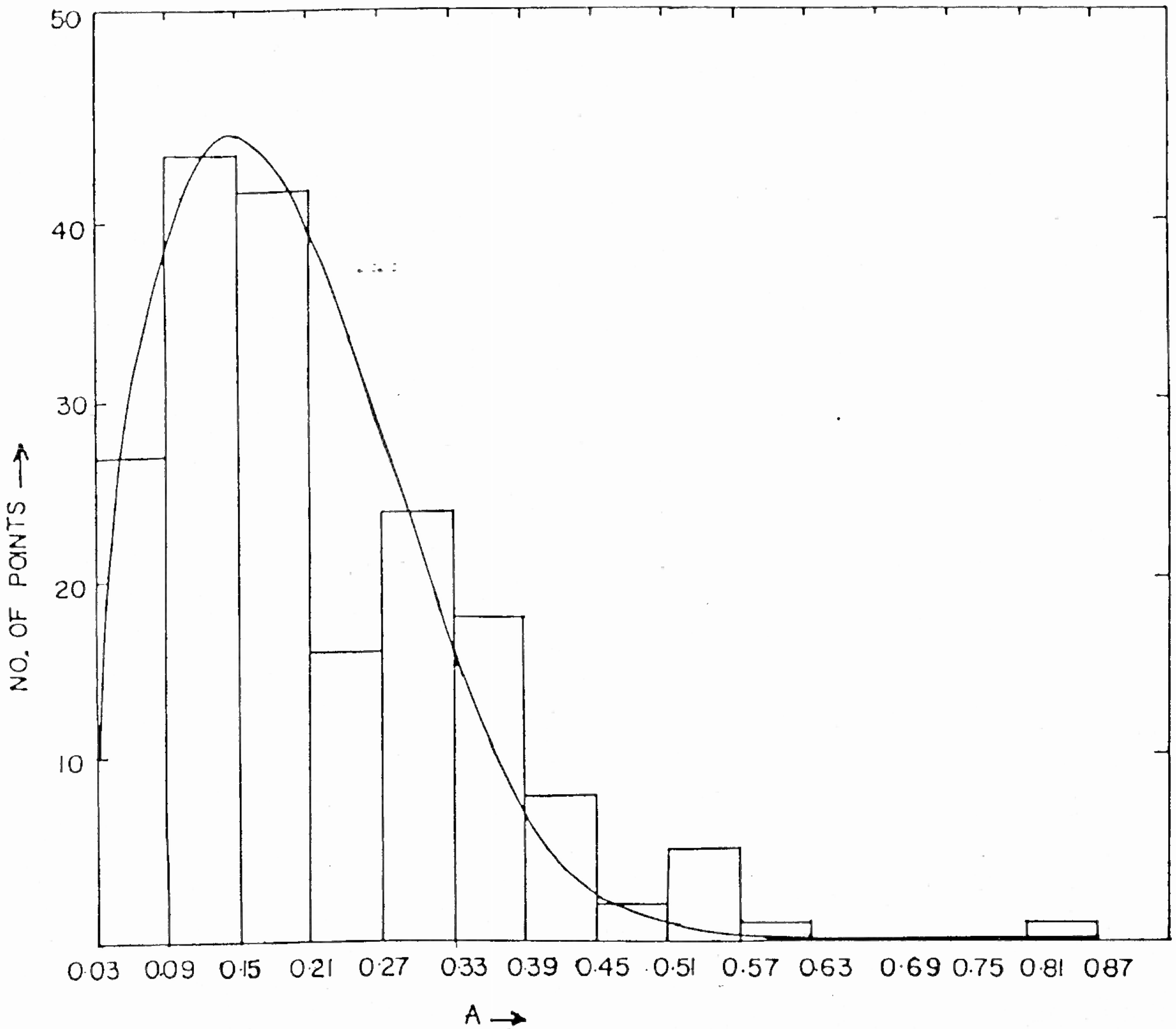


Fig. III-6: Frequency distribution of visibility amplitude in the absence of any strong source.

Figures III-5a and b, show $<|V_m|>/\sigma$ and $<|V_m|>/<|V_t|>$ respectively plotted as functions of the signal-to-noise ratio, $<|V_t|>/\sigma$. We have estimated the value of $\sigma$ by taking data with all the antennas tracking a 'blank' field (no source $\geq$ 0.7 Jy) and the diode phase-shifter values randomised so as not to form a beam. This leaves just the system noise at the correlator outputs. The frequency distribution of these visibility amplitudes ($A_N$) are plotted in Fig.III-6, after converting the counts into mJy using a calibration source. The continuous curve is the best-fit Rayleigh distribution of the form:

$$\rho(A_N) = K \frac{A_N}{\alpha^2} \exp\left[-\tfrac{1}{2} (A_N/\alpha)^2\right] \qquad \text{-------(3.6.3)}$$

The mean value of $A_N$ gives an estimate of the rms noise, $\sigma$ in the actual observing session. This has been obtained from the fitted value of $\alpha$, using the relation,

$$\bar{A}_N = \sqrt{\pi/2}\ \alpha \qquad \text{-------(3.6.4)}$$

The resulting value for the noise contribution is = 180 ± 94 mJy.

Hence, for a 1-Jy point source, the signal-to-noise ratio for each visibility point is ~ 5. From Fig.III-5b, we find that the positive noise bias in $<V_m>$ is then $\leq$ 2 % which is negligible compared to other uncertainties.

A further correction was included for the changes in the antenna gains for sources in the galactic plane introduced by the automatic level controller (ALC) at the input to the DDLC. We shall discuss this again in Chapter V.

(C) Most of the measurement errors come from the uncertainties in the

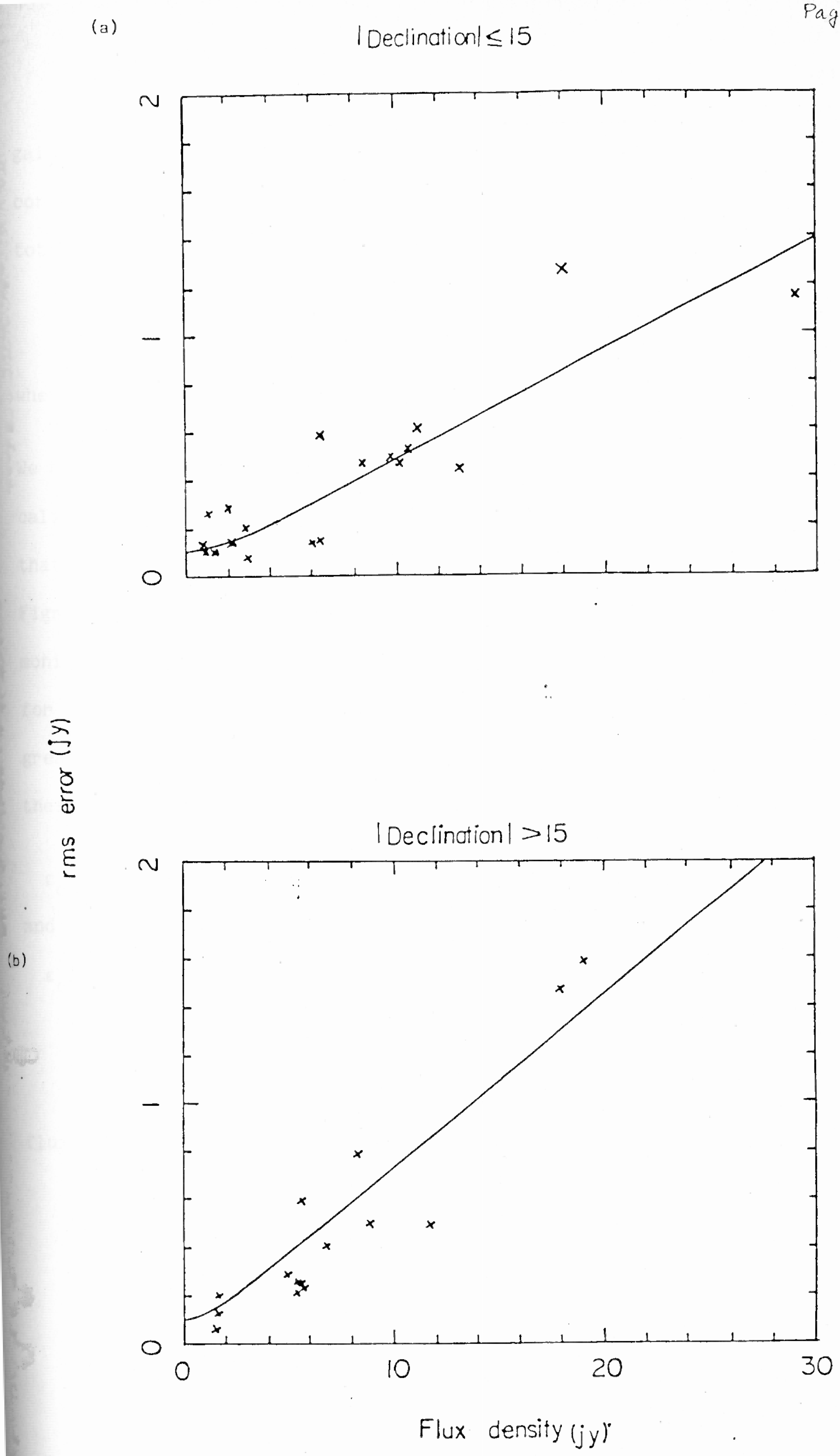


Fig. III-7a,b: Flux-density measurement errors in two declination ranges.

gain-declination fits, the calibration errors and the contribution of confusion (passage of background sources through the fringe pattern). The total error in Jy can be represented as:

$$\varepsilon_T^2 = \varepsilon_{con}^2 + (\varepsilon_{cal} \times S)^2 \qquad \text{-------(3.6.6)}$$

where, $\varepsilon_{cal}$ depends upon the declination of the source with flux density S.

We have obtained the values of $\varepsilon_{con}$ and $\varepsilon_{cal}$ from the observations of calibrators and control sources during the observing runs. It was found that sources at higher declinations had larger measurement errors. In Figs. III-7a and b, we have plotted the rms intensity fluctuations over a monitoring interval of three years (Chapter IV) versus the flux densities for the calibration and control sources with declinations less than and greater than 15° respectively. The above error-equation was fitted to these plots and the the values of the parameters were found to be:

$$\varepsilon_{con} = 0.1$$

and

$$\varepsilon_{cal} = 0.05 \text{ for } |\delta| \leq 15°$$

$$= 0.07 \text{ for } |\delta| > 15°$$

The method described in this chapter has been used for the flux-density measurements presented in Chapter IV and V.